Oxygen cluster anions revisited: Solvent-mediated dissociation of the core O_4^- anion

Dmitry Khuseynov, Daniel J. Goebbert,[a] and Andrei Sanov[b]
Department of Chemistry and Biochemistry, The University of Arizona, Tucson, Arizona 85721, USA

(Received 3 October 2011; accepted 13 February 2012; published online 7 March 2012)

The electronic structure and photochemistry of the $O_{2n}^-(H_2O)_m$, $n = 1$–6, $m = 0$–1 cluster anions is investigated at 532 nm using photoelectron imaging and photofragment mass-spectroscopy. The results indicate that both pure oxygen clusters and their hydrated counterparts with $n \geq 2$ form an O_4^- core. Fragmentation of these clusters yields predominantly O_2^- and $O_2^- \cdot H_2O$ anionic products, with the addition of O_4^- fragments for larger parent clusters. The fragment autodetachment patterns observed for O_6^- and larger O_{2n}^- species, as well as some of their hydrated counterparts, indicate that the corresponding O_2^- fragments are formed in excited vibrational states ($v \geq 4$). Yet, surprisingly, the unsolvated O_4^- anion itself does not show fragment autodetachment at 532 nm. It is hypothesized that the vibrationally excited O_2^- is formed in the intra-cluster photodissociation of the O_4^- core anion via a charge-hopping electronic relaxation mechanism mediated by asymmetric solvation of the nascent photofragments: $O_4^- \rightarrow O_2^-(X^2\Pi_g) + O_2(a^1\Delta_g) \rightarrow O_2(X^3\Sigma_g^-) + O_2^-(X^2\Pi_g)$. This process depends on the presence of solvent molecules and leads to vibrationally excited $O_2^-(X^2\Pi_g)$ products. © *2012 American Institute of Physics*. [http://dx.doi.org/10.1063/1.3691104]

I. INTRODUCTION

Experiments on cluster anions examine molecular-level interactions implicated in the chemistry of condensed environments.[1–3] Interactions of ions with solvent molecules perturb the electronic structure and may facilitate a variety of pathways and mechanisms for chemical reactions. This aspect of solvation plays a particularly important role for the reactions involving nonadiabatic transitions between electronic states.

Superoxide O_2^- and its clusters, particularly O_{2n}^-, have complicated photochemistry due to the existence of numerous low-lying electronic states. These clusters have long been considered perfect subjects for reaction dynamics studies, with several accounts of such studies available in the literature,[4–9] including particularly exhaustive investigations by Continetti and co-workers.[10,11] The experiments on both pure oxygen clusters, O_{2n}^-, and their hydrated counterparts, $O_{2n}^-(H_2O)_m$,[10,12,13] supported by theoretical studies,[14,15] showed that all species with $n \geq 2$ form an O_4^- core anion. The relatively high binding energy of O_2 to O_2^- (0.455 ± 0.22 eV) (Ref. 16) indicates partial covalent character in O_4^-.[5,10,14] As one specific example, the recent infrared spectra from the Johnson group[17] suggest the existence of two isomeric O_6^- structures, both corresponding to a mostly neutral O_2 solvent molecule bound to the O_4^- core. The O_4^- anion itself is described as two $O_2^{-1/2}$ moieties with weak covalent bonding between them.[10,14]

In our previous work,[12] we examined the effect of hydration on the oxygen cluster anions using photoelectron imaging and photofragment mass-spectroscopy of $[O_{2n}(H_2O)_m]^-$, $n = 1-4$, $m = 0-3$ at 355 nm. We confirmed that the identity of the O_4^- core anion is preserved for both the pure-oxygen and heterogeneously hydrated clusters with $n \geq 2$. Fragmentation of these clusters yielded predominantly the O_2^- and $O_2^-(H_2O)_l$, $l < m$, anionic products, while the presence of low-electron kinetic energy autodetachment features in the photoelectron images indicated that the fragments were vibrationally excited.

In the present work, we extend our previous study[12] and report photoelectron spectra and anionic photofragmentation pathways of $[O_{2n}(H_2O)_m]^-$, $n = 1-6$, $m = 0-1$ at 532 nm. This wavelength is particularly important in understanding the photodynamics, because the only dissociation channel in the core O_4^- accessible in this regime yields vibrationally cold $O_2^-(X^2\Pi_g)$ and electronically excited $O_2(a^1\Delta_g)$.[8,9] In a cluster environment, these nascent products may undergo nonadiabatic transitions leading to the opening of the electronically relaxed reaction channel. These transitions and the overall effect of solvation on the photochemistry of these clusters are the primary focus of this work. As in the previous work,[10,12] we observe intense autodetachment bands for O_6^- and larger O_{2n}^- parent anions, as well as some of their hydrated counterparts. Autodetachment is attributed to vibrationally excited ($v \geq 4$) O_2^- fragments formed along the electronically relaxed core dissociation asymptote. In order to explain the experimental observations, we propose a charge-hopping mechanism for electronic-to-vibrational energy transfer, mediated by asymmetric solvation of the nascent $O_2^-(X^2\Pi_g) + O_2(a^1\Delta_g)$ photofragments of the core O_4^- anion.

[a]Present address: Department of Chemistry, The University of Alabama, Tuscaloosa, Alabama 35487, USA
[b]Electronic mail: sanov@u.arizona.edu.

II. EXPERIMENTAL SECTION

The experiments were performed using a pulsed reflectron time-of-flight mass-spectrometer equipped with a photoelectron velocity-map[18] imaging[19,20] detector that has been described in detail in Ref. 21.

Neat O_2 gas with 20 psi backing pressure was expanded into a high-vacuum chamber through a pulsed supersonic nozzle (General Valve Series 9), operated at a 50 Hz repetition rate. Cluster ions were synthesized by secondary electron attachment upon interaction of the gas jet with a 1 keV electron beam. The anions were accelerated to a kinetic energy of about 3 keV and focused on a laser interaction region, where the ion beam was crossed with a linearly polarized pulsed laser beam. The second harmonic of the Nd:YAG (yttrium aluminum garnet) laser was used to produce 532 nm radiation with an 8 ns pulse width and a 20–30 mJ/pulse power. Parent ions were detected using a microchannel plate (MCP) detector (Burle, Inc.) mounted at the end of flight tube. Two types of experiments were performed in the laser interaction region: photoelectron imaging and photofragmentation.

In the imaging measurements, electrons were projected onto a 40 mm diameter MCP detector coupled with a phosphor screen (Burle, Inc.) using static electric fields within the velocity-map imaging assembly. Images were recorded with 1 megapixel charge-coupled device camera and were typically accumulated for $\sim 10^4 - 10^5$ experimental cycles. Kinetic energy and angular distributions of the photodetached electrons were obtained via inverse Abel transform[20,22] as implemented in the BASEX program.[23] The kinetic energy scale was calibrated using the well-known photodetachment transition of O^-.[24,25]

Photofragment ions were detected by using a single-stage linear-field reflectron. Parent ions with mass m_p were initially refocused to the off-axis MCP detector and the signal was optimized by varying the reflectron potential V_p. Fragment ions with mass m_f can be then focused on the same off-axis detector, with the same arrival time as the parent ions, by reducing the reflectron voltage to $V_f = V_p(m_f/m_p)$. Photofragment mass-spectra were recorded by scanning reflectron potential.

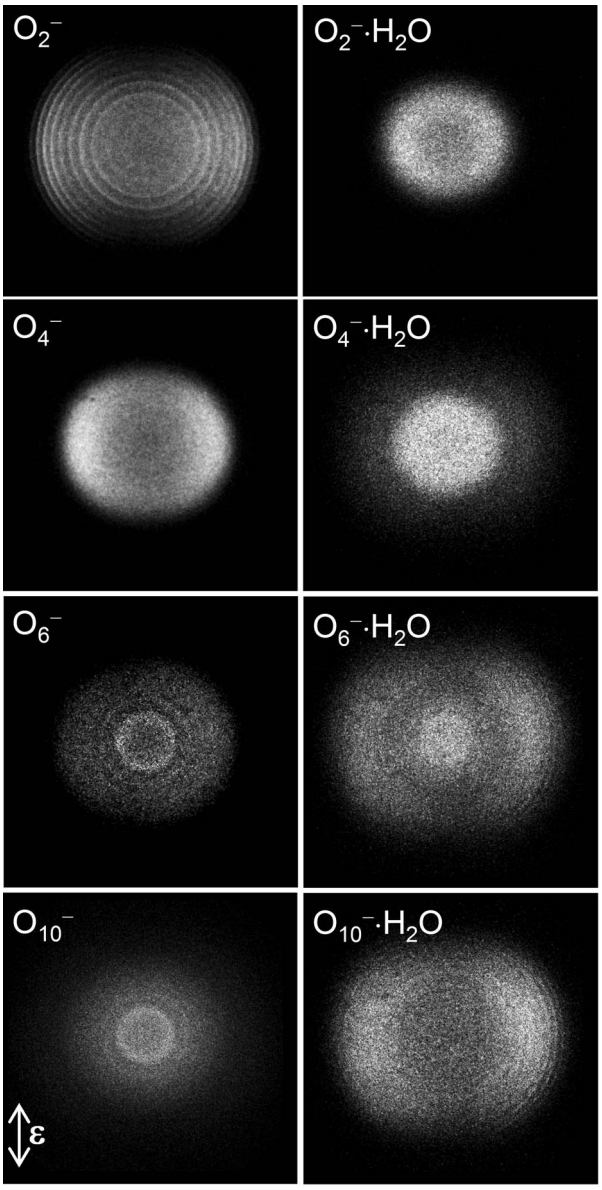

FIG. 1. 532 nm photoelectron images of representative $O_{2n}^-(H_2O)_m$ clusters anions. All images were recorded under the same experimental conditions and shown on the same velocity scales.

III. RESULTS

A. Photoelectron imaging spectroscopy

Photoelectron images of the $[O_{2n}(H_2O)_m]^-$, n = 1–6, m = 0–1 cluster anions were recorded using linearly polarized 532 nm radiation. Figure 1 shows several representative images, corresponding to the pure and monohydrated O_2^-, O_4^-, O_6^-, and O_{10}^- ions. The photoelectron spectra obtained from all images recorded in this study, including those shown in Figure 1, are presented in Figure 2. The spectra are plotted versus electron binding energy (eBE), calculated from electron kinetic energy (eKE) as eBE = $h\nu$ − eKE.

The two well-resolved progressions A and B in the photoelectron spectrum of O_2^- are attributed to vibrations in the ground and first excited electronic states of neutral O_2, the $X^3\Sigma_g^-$ and $a^1\Delta_g$ states, respectively.[26] The vibrational structure of both electronic bands is also apparent in the raw photoelectron image of O_2^- shown in Figure 1. As both bands have been the subjects of several previous investigations,[7,8,12,26–29] they will not be discussed here. The broad bands in the photoelectron spectra of O_4^-, O_6^-, and O_8^- (Figure 2) are attributed to direct dissociative photodetachment of the O_4^- core of these clusters via the overall $O_4^- \rightarrow 2O_2(X^3\Sigma_g^-) + e^-$ pathway.[8,10,12,30] Similar to the first band in the O_2^- spectrum, these bands are labeled A, because they too correspond to the formation of O_2 molecules in the ground electronic state. The higher energy dissociative photodetachment channel, $O_4^- \rightarrow O_2(X^3\Sigma_g^-) + O_2(a^1\Delta_g) + e^-$, is not observed at 532 nm (Figure 2), as it was in the 355 nm spectrum.[8,12]

The maximum of band A in the O_4^- spectrum is shifted to higher binding energy, relative to the most intense O_2^- peak, by ∼0.6 eV, as indicated by the green horizontal arrow in Figure 2. The shift reflects the approximate O_4^-

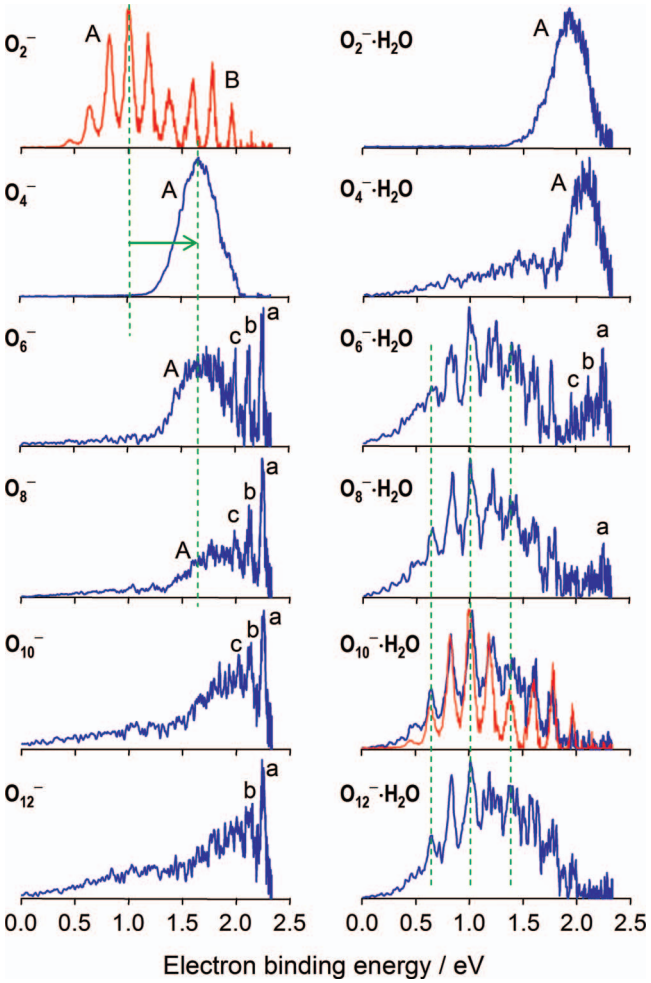

FIG. 2. 532 nm photoelectron spectra of $[O_{2n}(H_2O)_m]^-$, $n = 1$–6, $m = 0$–1 obtained from the images shown in Figure 1. Labels A and B correspond to the formation of O_2 in the ground $X^3\Sigma_g^-$ or first excited $a^1\Delta_g$ states, respectively, via direct photodetachment (for $n = 1$) or O_4^- dissociative photodetachment (for $n \geq 2$).

$\rightarrow O_2(X^3\Sigma_g^-) + O_2^-(X^2\Pi_g)$ dissociation energy and its magnitude is indicative of the weakly covalent bonding character between two diatomic moieties in O_4^-.[12,14,15,31] The much smaller shift of band A in the O_6^- spectrum, compared to O_4^-, is attributed to electrostatic solvation interactions in the $O_4^-(O_2)_{n-2}$, $n > 2$ structures.

In the spectra of O_6^- and larger O_{2n}^- clusters (Figure 2), we observe series of sharp low-eKE peaks labeled with lower case letters (a, b, ...). These peaks correspond to the well-defined isotropic rings near the respective image centers (see, for example, the O_6^- and O_{10}^- images in Figure 1). These features are assigned to autodetachment of vibrationally excited O_2^- photofragments.[10,12]

The effect of a single water molecule on electron photoemission can be seen in the right columns of Figures 1 and 2, where the results for the $O_{2n}^- \cdot H_2O$ clusters are presented. Two intriguing aspects of these results are immediately apparent. First, the autodetachment features a–c are markedly weaker or altogether absent for the monohydrated clusters. Second, the photoelectron intensity for the larger species, for example, $O_6^- \cdot H_2O$ and $O_{10}^- \cdot H_2O$, is spread over greater effective images areas, compared to the smaller clusters, such as $O_2^- \cdot H_2O$. (All photoelectron images in Figure 1 are shown on the same velocity scale.) This visually striking observation is counterintuitive, as under otherwise unchanged conditions one expects the average eKE and hence the effective areas of photoelectron images to decrease with increasing cluster size, due to solvation-induced stabilization of the cluster anions.[1,3] The larger effective image areas reflect the presence of higher eKE spectral bands, which upon close examination can be seen in the images of all larger clusters studied in this work: O_{2n}^-, $n \geq 4$, and $O_{2n}^- \cdot H_2O$, $n \geq 3$.

These bands are particularly prominent in the hydrated cluster-anion images and spectra, $O_{2n}^- \cdot H_2O$, $n \geq 3$. For these species, the bands in question are vibrationally resolved (Figure 2) and exhibit predominantly perpendicular photoelectron angular distributions (Figure 1). The observed vibrational pattern and the characteristic angular distributions are fingerprints of O_2^- photodetachment. To stress this conclusion, the photoelectron spectrum of $O_{10}^- \cdot H_2O$, shown in the corresponding panel of Figure 2 in blue, is superimposed with the spectrum of O_2^- (red), reproduced from the top-left panel of the figure. The agreement between the larger eKE $O_{10}^- \cdot H_2O$ band and the O_2^- spectrum is unmistakable. Therefore, the high-eKE/low-eBE bands in the photoelectron spectra of O_{2n}^-, $n \geq 4$, and $O_{2n}^- \cdot H_2O$, $n \geq 3$, are attributed to the photodetachment of O_2^- formed in the photofragmentation of the respective parent clusters, a net two-photon process. This conclusion was further supported by photoelectron imaging results for the same ion obtained using two different laser fluences, 0.8×10^{-4} and 1.2×10^{-4} W/cm^2 (data not shown here). The image taken with higher laser power shows significant increase in the relative O_2^- photodetachment bands' intensity, consistent with a two-photon process.

B. Photofragment mass-spectroscopy

The same series of mass-selected anions, $[O_{2n}(H_2O)_m]^-$, $n = 2$–6, $m = 0$ and 1, was studied using photofragment mass-spectroscopy. The 532 nm spectra are presented in Figure 3. For the unhydrated ($m = 0$) O_{2n}^-, $n = 2$–5, species, O_2^- is the only anionic photofragment observed, with O_4^- appearing for $n = 6$. The monohydrated ($m = 1$) clusters studied yield both O_2^- and $O_2^- \cdot H_2O$. The branching ratio of these fragments varies from cluster to cluster, as evident in Figure 3, albeit not dramatically. In addition, the $O_{2n}^- \cdot H_2O$ clusters with $n \geq 4$ yield small but detectable quantities of O_4^- photofragments.

IV. DISCUSSION

In addition to direct dissociative photodetachment (band A), the photoelectron spectra of pure-oxygen clusters O_{2n}^-, $n \geq 3$, as well as some of their monohydrated counterparts, $O_{2n}^- \cdot H_2O$, display low-eKE features (peaks a–c in Figure 2). These peaks correspond to isotropic rings close to the centers of the photoelectron images (Figure 1). Their spectral positions do not shift as a result of solvation by O_2 or hydration. These properties are signs of an indirect detachment process and we assign features a–c to autodetachment from

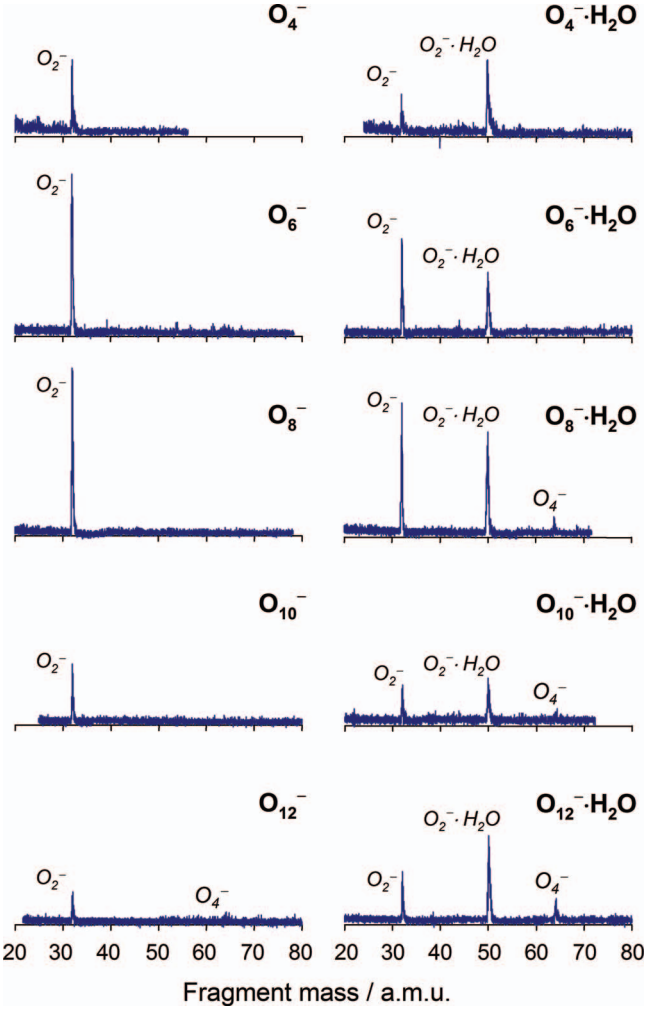

FIG. 3. 532 nm photofragmentation mass spectra for $O_{2n}^-(H_2O)_m$, $n = 2$–6, $m = 0$–1. The parent clusters are indicated in bold in the upper right corners of the corresponding spectral panels, while the fragment peaks are labeled in *italics*. The spectra were recorded at the same detector voltages and are presented on consistent intensity scales.

O_2^- photofragments. Similar features have been observed by Continetti and co-workers at 355 and 532 nm,[10] as well as in our previous work at 355 nm.[12]

The assignment of the autodetachment features to O_2^- fragments is further (indirectly) supported by the photofragmentation data presented in Figure 3. For the O_{2n}^-, $n \geq 3$ series, O_2^- is the only anionic fragment observed at 532 nm. At the same time, progressions of O_2^- autodetachment features a–c are prominent in the corresponding photoelectron spectra (Figure 2). For the hydrated series, $O_{2n}^- \cdot H_2O$, $n \geq 3$, the O_2^- fragment branching ratio decreases with increasing n, which parallels the disappearance of the autodetachment features in the $O_{10}^-(H_2O)$ and $O_{12}^-(H_2O)$ photoelectron spectra.

We will focus on one key result of this work, expanding on the previous observations by Continetti and co-workers,[10,11] namely, the intense autodetachment of O_2^- fragments observed for O_6^- and larger O_{2n}^- species at 532 nm, contrasting its marked absence for O_4^-. This result is seemingly at odds with another experimental fact, that O_2^- photofragments are produced for all of these parent ions (Figure 3). Similar experiments at 355 nm do show significant fragment autodetachment signal for O_4^-, but the autodetachment yield is surprisingly enhanced for O_6^-.[10,12]

Autodetachment is expected for vibrationally excited O_2^- fragments, since the vibrational levels with $v \geq 4$ lie higher in energy than the ground electronic and vibrational state of neutral O_2.[5,10] The above observations suggest that at both 355 and 532 nm the O_2^- fragments, on average, have a higher degree of internal (vibrational) excitation when they are formed from O_6^-, via an overall $O_6^- \rightarrow O_2^- + 2O_2$ process, compared to the $O_4^- \rightarrow O_2^- + O_2$ dissociation. This conclusion contrasts statistical expectations, since O_6^- dissociation involves more degrees of freedom, compared to O_4^-.

Based on the previous experimental[5,10–12] and theoretical[14,15] studies, the O_{2n}^- and $O_{2n}^- \cdot H_2O$, $n \geq 2$ species are well described as covalently bound O_4^- anions, solvated by the remaining neutral molecules. The O_4^- anion is, in turn, described as two $O_2^{-1/2}$ moieties with weak covalent bonding between them, arranged in a rectangular (D_{2h}) structure shown in Figure 4(b).[10,14] In this structure, corresponding to the X^2A_u electronic state, the excess electron is shared between the respective $\pi_g^*(2p)$ orbitals

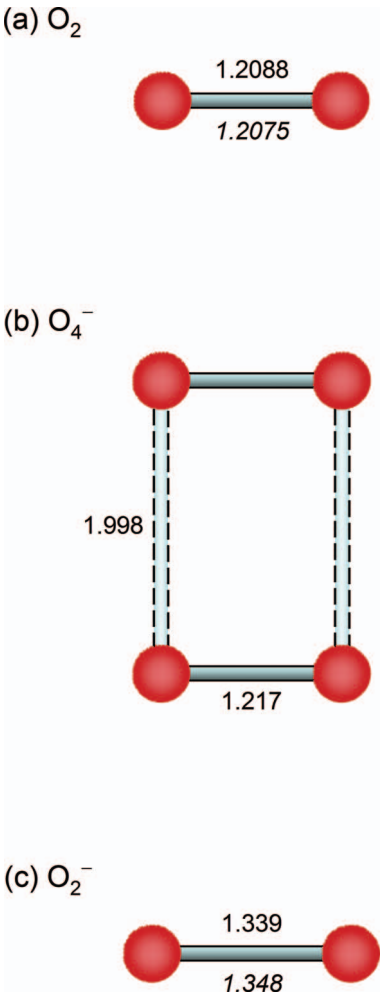

FIG. 4. The equilibrium structures of (a) O_2, (b) O_4^-, and (c) O_2^-. Bond lengths are indicated in Ångstroms. The Roman-type values are from CCSD(T)/aug-cc-pVTZ calculations. For comparison, the numbers in italics are experimental measurements (Refs. 38 and 39 for O_2 and Ref. 26 for O_2^-). The O_4^- structure is from Ref. 14.

of the two equivalent diatomic moieties.[14] The antibonding character of $\pi_g^*(2p)$ is responsible for the greater bond length in O_2^-, compared to neutral O_2 [Figures 4(a) and 4(c)]. Delocalizing the additional $\pi_g^*(2p)$ electron between two $O_2^{-1/2}$ moieties in O_4^- should lead to each of the $O_2^{-1/2}$ bonds being shorter than the O_2^- bond.

Based on this qualitative expectation alone, one might propose a naive explanation for the enhanced vibrational excitation and, hence, autodetachment of O_2^- photofragments ejected from O_6^-, compared to those resulting from unsolvated O_4^- dissociation. The extent of charge delocalization in O_6^-, even though it is described as nominally $O_4^- \cdot O_2$, is likely to be more significant than in O_4^-. That is, a more appropriate description for O_6^- might be $O_2^{-(1-\delta)/2}O_2^{-(1-\delta)/2}O_2^{-\delta}$, with $0 < \delta \ll 1$. The reduced populations of the diatomic antibonding $\pi_g^*(2p)$ orbitals in the core anion should translate into shorter O–O bonds, which, in turn, would result in a greater geometry change imparted on an O_2^- fragment ejected impulsively from O_6^-. This would be consistent with a greater degree of O_2^- fragment vibrational excitation and, hence, autodetachment in the O_6^- case, compared to O_4^-.

However, the $O_2^{-1/2}$ bond length in O_4^- is predicted to be much closer to that in neutral O_2 than in O_2^- (see Figure 4), indicating that the excess electron in O_4^- contributes mainly to the bonding between the two $O_2^{-1/2}$ moieties. Therefore, further charge delocalization in O_{2n}^-, $n \geq 3$ can result in only a miniscule reduction in the $O_2^{-(1-\delta)/2}$ bond length. Such a small geometry change cannot explain the drastic difference in the 532 nm fragment autodetachment channel in O_6^- versus O_4^-. A more detailed analysis of the electronic structure is, therefore, required to explain the experimental observations.

The ground state of O_4^- as well as its first two excited states, A^2B_{3g} and B^2B_{2g}, correlate asymptotically with the lowest $O_2(X^3\Sigma_g^-) + O_2^-(X^2\Pi_g)$ dissociation limit.[10,14] However, 532 nm excitation from the X^2A_u state accesses the higher lying $^2B_{3g}$ state, C^2B_{3g}, which correlates to the electronically excited $O_2(a^1\Delta_g) + O_2^-(X^2\Pi_g)$ channel.[14] At the CASSCF/ICCI level of theory,[14] there is a large vertical energy gap (1.77 eV) between the two $^2B_{3g}$ states.

In agreement with these predictions, the only anionic photodissociation pathway in O_4^- observed in this wavelength region yields vibrationally cold $O_2^-(X^2\Pi_g)$ and electronically excited $O_2(a^1\Delta_g)$.[8,9] Specifically, 86% of the O_2^- products at 523.6 nm are formed in the ground vibrational state, with 14% in $v = 1$.[8] Hence, most available energy in O_4^- photodissociation in this regime is tied up in the electronic excitation of O_2.

At shorter wavelength, both the $O_2^-(X^2\Pi_g) + O_2(a^1\Delta_g)$ and $O_2^-(X^2\Pi_g) + O_2(X^3\Sigma_g^-)$ channels are accessed in O_4^- dissociation, with the latter channel resulting in vibrationally hot (autodetaching) anionic products.[8,9,12] It has been suggested that the very specific energy partitioning observed in the vicinity of 532 nm may be driven by an O_4^- vibronic resonance.[9,32] Away from this possible resonance, O_4^- dissociation is less state specific, accessing a broader range of available electronic and vibrational product channels. In our past work, for example, this manifested in the appearance of fragment autodetachment peaks in the unsolvated O_4^- spectra at 355 nm.[12] However, the mere increase in the total available energy at 355 vs. 532 nm may also result in the formation of vibrationally excited O_2^- products, even in coincidence with electronically excited O_2.[8]

The above $O_4^- + 532\text{ nm} \rightarrow O_2^-(X^2\Pi_g) + O_2(a^1\Delta_g)$ channel is largely preserved in O_6^-, despite the presence of a third O_2 moiety.[11] However, the O_6^- cluster anion also exhibits the electronically relaxed channel, not observed for O_4^- at this wavelength. Namely, in the O_6^- cluster, the core O_4^- dissociates into $O_2^-(X^2\Pi_g) + O_2(X^3\Sigma_g^-)$ with significant population of higher vibrational level of O_2^- ($v \geq 4$), and the overall cluster process described as $O_6^- \rightarrow O_2^-(X^2\Pi_g) + 2O_2(X^3\Sigma_g^-)$. This pathway leads to autodetachment from the vibrationally excited O_2^- fragments, as seen both in the past work[5,10–12] and the results presented here (features a–c in Figure 2).

These findings indicate nonadiabatic transitions between the $O_4^- \rightarrow O_2(a^1\Delta_g) + O_2^-(X^2\Pi_g)$ and $O_2^-(X^2\Pi_g) + O_2(X^3\Sigma_g^-)$ dissociation asymptotes occurring in the presence of solvent molecules (i.e., in O_6^- and larger O_{2n}^- clusters). Such relaxation amounts to electronic-vibrational energy transfer, leaving a measurable fraction of the anionic fragments in vibrationally excited, autodetaching states ($v \geq 4$). Several explanations for the drastic change in the dissociation dynamics of O_6^-, compared to O_4^-, have been put forth, including a charge-transfer-to-solvent model, solvent-induced nonadiabatic coupling of the core O_4^- anion electronic states, and caging.[5,10]

Each of these mechanisms may contribute to the dissociation process and none can be clearly singled out. Based on the recent advances in cluster chemistry, we propose yet another, complementary view of the O_{2n}^- and $O_{2n}^- \cdot H_2O$, $n \geq 3$, dissociation process. Namely, the electronic excitation of the nascent fragments of the core O_4^- anion in 532 nm dissociation via the C^2B_{3g} state,[9,14] may be transferred to the vibrational degrees of freedom by means of charge transfer from the nascent O_2^- to the counter fragment, the electronically excited O_2.

This mechanism is described as an overall $O_4^-(C^2B_{3g}) \rightarrow O_2^-(X^2\Pi_g) + O_2(a^1\Delta_g) \rightarrow O_2(X^3\Sigma_g^-) + O_2^-(X^2\Pi_g)$ process involving the nascent core photofragments. Similar solvent-assisted mechanisms were previously proposed for other in-cluster fragmentation processes, such as the spin-orbit quenching of $I(^2P_{1/2})$ photofragments of I_2^- photodissociation at 395 nm via an $I^- + I(^2P_{1/2}) \rightarrow I(^2P_{3/2}) + I^-$ mechanism (Refs. 33–35) and $I^- + Br \rightarrow I + Br^-$ relaxation of IBr^- dissociation products in the presence of CO_2.[36,37]

The electron-hopping process proposed for the present case is illustrated at the molecular-orbital level in Figure 5(a), where the initial and final populations of the doubly degenerate $\pi_g^*(2p)$ HOMOs of both diatomic fragments (O_2^- and O_2) are shown, corresponding to the nascent $O_2^-(X^2\Pi_g) + O_2(a^1\Delta_g)$ fragments of $O_4^-(C^2B_{3g})$ dissociation on the left and the electron-hopping products, $O_2(X^3\Sigma_g^-) + O_2^-(X^2\Pi_g)$, on the right.

Energetically, the charge-transfer is made possible by asymmetric solvation in the cluster environment, as illustrated in the qualitative diagram in Figure 5(b). For given internal

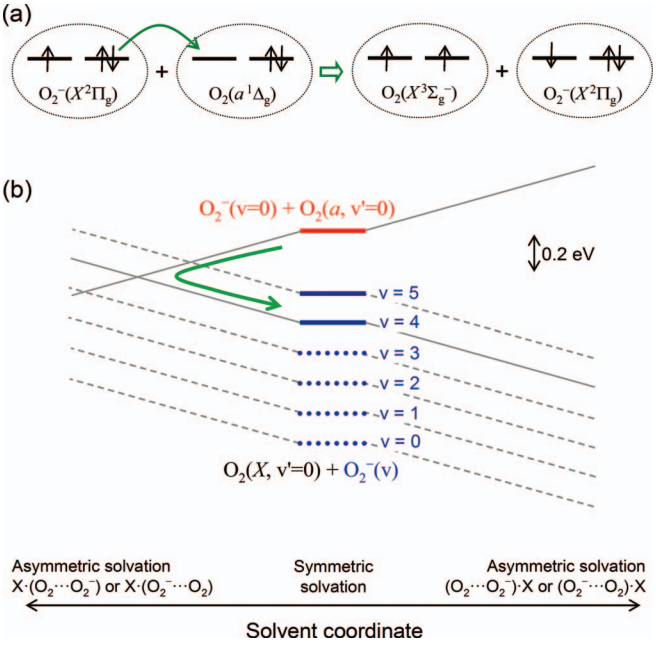

FIG. 5. (a) Molecular-orbital level illustration of the $O_2^-(X^2\Pi_g) + O_2(a^1\Delta_g) \rightarrow O_2(X^3\Sigma_g^-) + O_2^-(X^2\Pi_g)$ relaxation process via electron-hopping. The initial and final populations of the doubly degenerate $\pi_g^*(2p)$ HOMOs of O_2^- and O_2 are shown, corresponding to the nascent fragments of O_4^- dissociation on the left and the electron-hopping products on the right. (b) Illustration of the proposed electron-hopping mechanism, induced by asymmetric solvation. The vertical double arrow shows the approximate energy scale of the diagram. See the text for details.

states, the $O_2^- \cdots O_2$ and $O_2 \cdots O_2^-$ fragment pairs are degenerate only in the absence of solvent or in a symmetric solvent environment. In the more common case of asymmetric solvation, the fragment pair corresponding to a more solvated anion will, in general, be more stable than the same pair (same internal states) with the solvent in closer proximity to the neutral fragment.

For the purpose of illustration, let $X\cdot(O_2^- \cdots O_2)$ represent asymmetric solvation of the $O_2^- \cdots O_2$ fragment pair with neutral solvent molecules X preferentially located on the anion, O_2^-, side. The $X\cdot(O_2^- \cdots O_2)$ state is degenerate with its mirror-image counterpart, the $(O_2 \cdots O_2^-)\cdot X$ state, which is obtained by inversion of the coordinates of all nuclei and electrons in the system. However, should charge transfer occur in either of these two states without change in the solvent configuration, a transition described as $X\cdot(O_2^- \cdots O_2) \rightarrow X\cdot(O_2 \cdots O_2^-)$ or $(O_2 \cdots O_2^-)\cdot X \rightarrow (O_2^- \cdots O_2)\cdot X$, respectively, the energy of the cluster will increase in both cases (assuming the internal states of the "new" O_2 and O_2^- are the same as those of the initial respective species).

In general, the energy of a fragment pair is dependent not only on the O_2 and O_2^- internal states, but also on solvation asymmetry or the "solvent coordinate." In the above illustration, the opposite directions along this coordinate correspond to the $X\cdot(\dots)$ and $(\dots)\cdot X$ solvent configurations, which we shall refer to, for brevity, as "left" and "right." The overall state of the solvated pair is thus described by both the charge localization, $O_2^- \cdots O_2$ or $O_2 \cdots O_2^-$, and the solvent coordinate, ranging from $X\cdot(\dots)$ to $(\dots)\cdot X$.

As illustrated pictorially in Figure 5(b), the $O_2^- \cdots O_2$ pair energy increases along the solvent coordinate from left to right, i.e., from $X\cdot(O_2^- \cdots O_2)$ to $(O_2^- \cdots O_2)\cdot X$, while the opposite is true for $O_2 \cdots O_2^-$. Specifically, Figure 5(b) illustrates asymmetric solvation of the nascent $O_2^-(X^2\Pi_g, v = 0) + O_2(a^1\Delta_g, v' = 0)$ fragment pair and several charged-switched, electronically relaxed $O_2(X^3\Sigma_g^-, v' = 0) + O_2^-(X^2\Pi_g, v = 0\text{–}5)$ states. The energy of the former pair increases along the solvent coordinate from left to right, i.e., from $X\cdot(O_2^- \cdots O_2)$ to $(O_2^- \cdots O_2)\cdot X$, while the energy of each of the latter charge-switched states decreases in the same direction.

In explaining the observed O_2^- autodetachment, we are concerned with the formation of $O_2^-(X^2\Pi_g, v \geq 4)$ photofragments. The green arrow in Figure 5(b) indicates a possible pathway, specifically for the formation of O_2^- in $v = 4$: $O_2^-(X^2\Pi_g, v = 0) + O_2(a^1\Delta_g, v' = 0) \rightarrow O_2(X^3\Sigma_g^-, v' = 0) + O_2^-(X^2\Pi_g, v = 4)$. In the absence of solvent (or for symmetric solvation), the energy gap between the initial and final states of this process is in excess of 0.4 eV. The corresponding gaps are smaller for higher vibrationally excited final states, but even the $v = 4$ gap, indicated in Figure 5(b), can be bridged for certain solvent configurations on the left side of the solvent-coordinate axis. It could be argued that just one solvating O_2 molecule might not be sufficient to achieve an $O_2^-(X^2\Pi_g, v = 0) + O_2(a^1\Delta_g, v' = 0)$ and $O_2(X^3\Sigma_g^-, v' = 0) + O_2^-(X^2\Pi_g, v = 4)$ resonance in the O_6^- cluster dissociation. However, due to the large geometry difference between O_2 and O_2^- (see Figure 4), both O_2 and O_2^- fragments are likely to be vibrationally excited as a result of an $O_2^- + O_2 \rightarrow O_2 + O_2^-$ charge hopping. Vibrational excitation shifts the $O_2(X^3\Sigma_g^-, v' > 0) + O_2^-(X^2\Pi_g, v)$ levels in Figure 5(b) to higher energies, making the described electron-hopping transitions more plausible, particularly for highly vibrationally excited final states.

The proposed pathway leads to vibrationally excited $O_2^-(X^2\Pi_g)$ products, as the initial electronic excitation of O_2 is converted to vibrational excitation of O_2^- (same molecular moiety). The vibrational excitation of O_2^- is manifest as autodetachment bands in the photoelectron data, as the $O_2^-(X^2\Pi_g, v \geq 4)$ levels are embedded in the detachment continuum. This pathway is due to dissociating O_4^- interacting with the solvent. As might be expected, it does not take over the dissociation process completely, but competes with the "original," electronically excited but vibrationally cold $O_2^-(X^2\Pi_g) + O_2(a^1\Delta_g)$ channel (the only channel in 532 nm dissociation of unsolvated O_4^-).

We finally note that the greatest fragment autodetachment intensity, relative to the direct photodetachment bands, is observed for O_{2n}^-, $n \geq 3$. The autodetachment is significantly weaker for the hydrated $O_{2n}^- \cdot H_2O$ species (see Figure 2), consistent with the greater solvation-induced stabilization in these clusters, which is due to the high solvent binding energy of water (~0.7 eV), compared to O_2 (~0.1 eV).[12] It is, however, intriguing that no clear autodetachment signatures are observed for $O_4^- \cdot H_2O$, while the $O_6^- \cdot H_2O$ spectrum does show autodetachment peaks (see the right column in Figure 2). Combined with the results for the unhydrated O_{2n}^- cluster anions (left column in Figure 2), this observation

suggests that at least one solvent O_2 molecule is necessary for fragment autodetachment to occur, while a single H_2O by itself does not have the same effect. This may be due to the particulars of the corresponding cluster structures (if, for example, H_2O binds to O_4^- in a symmetric manner, while O_2 does not). It seems, however, more likely that a solvent O_2, due to its chemical nature and positive electron affinity, plays a more direct role in the proposed electron-hopping process, possibly acting as a transfer bridge between the nascent $O_2^- \cdots O_2$ fragments. A similar role was proposed recently for CO_2 mediating the fragment relaxation process in $IBr^- \cdot CO_2$ dissociation.[36,37] Time-resolved measurements on some of the $O_{2n}^-(H_2O)_m$ clusters, particularly on O_6^-, would go a long way to either confirm or disprove this speculation.

V. CONCLUSIONS

The electronic structure and photochemistry of $O_{2n}^-(H_2O)_m$, $n = 1$–6, $m = 0$–1 cluster anions has been investigated using photoelectron imaging and photofragment mass-spectroscopy at 532 nm. Both pure oxygen clusters and their hydrated counterparts with $n \geq 2$ form an O_4^- core anion. Fragmentation of these clusters yields predominantly O_2^- and $O_2^- \cdot H_2O$ anionic products, with the addition of O_4^- fragments for larger clusters. The fragment autodetachment patterns observed for O_6^- and larger O_{2n}^- species, as well as some of their hydrated counterparts, indicate that the corresponding O_2^- fragments are formed in excited vibrational states ($v \geq 4$). Yet surprisingly, the unsolvated O_4^- anion itself does not show fragment autodetachment. Excitation at 532 nm promotes the core O_4^- anion to a dissociative state that leads to the $O_2^-(X^2\Pi_g) + O_2(a^1\Delta_g)$ dissociation channel. It is hypothesized that in a cluster environment, interaction with the solvent results in nonadiabatic electronic quenching of the nascent fragment pair via a charge-hopping mechanism $O_2^-(X^2\Pi_g) + O_2(a^1\Delta_g) \rightarrow O_2(X^3\Sigma_g^-) + O_2^-(X^2\Pi_g)$. This process, mediated by solvent asymmetry and possibly a bridging role played by solvent O_2 molecules, leads to vibrationally excited $O_2^-(X^2\Pi_g)$ products.

ACKNOWLEDGMENTS

This work is supported by the U.S. National Science Foundation (Grant No. CHE-1011895). D.K. would also like to thank the State of Arizona TRIF Imaging Fellowship program for partial support.

[1] A. W. Castleman and K. H. Bowen, J. Phys. Chem. **100**, 12911 (1996).
[2] A. Sanov and W. C. Lineberger, PhysChemComm **5**, 165 (2002).
[3] A. Sanov and W. C. Lineberger, Phys. Chem. Chem. Phys. **6**, 2018 (2004).
[4] L. A. Posey, M. J. DeLuca, and M. A. Johnson, Chem. Phys. Lett. **131**, 170 (1986).
[5] M. J. DeLuca, C.-C. Han, and M. A. Johnson, J. Chem. Phys. **93**, 268 (1990).
[6] C. R. Sherwood, M. C. Garner, K. A. Hanold, K. M. Strong, and R. E. Continetti, J. Chem. Phys. **102**, 6949 (1995).
[7] C. R. Sherwood and R. E. Continetti, Chem. Phys. Lett. **258**, 171 (1996).
[8] C. R. Sherwood, K. A. Hanold, M. C. Garner, K. M. Strong, and R. E. Continetti, J. Chem. Phys. **105**, 10803 (1996).
[9] K. A. Hanold and R. E. Continetti, Chem. Phys. **239**, 493 (1998).
[10] R. J. Li, K. A. Hanold, M. C. Garner, A. K. Luong, and R. E. Continetti, Faraday Discuss. **108**, 115 (1997).
[11] K. A. Hanold, A. K. Luong, and R. E. Continetti, J. Chem. Phys. **109**, 9215 (1998).
[12] D. J. Goebbert and A. Sanov, J. Chem. Phys. **131**, 104308 (2009).
[13] V. Y. Antonchenko and E. S. Kryachko, J. Phys. Chem. A **109**, 3052 (2005).
[14] A. J. A. Aquino, P. R. Taylor, and S. P. Walch, J. Chem. Phys. **114**, 3010 (2001).
[15] D. C. Conway, J. Chem. Phys. **50**, 3864 (1969).
[16] K. Hiraoka, J. Chem. Phys. **89**, 3190 (1988).
[17] J. C. Bopp, A. N. Alexandrova, B. M. Elliott, T. Herden, and M. A. Johnson, Int. J. Mass Spectrom. **283**, 94 (2009).
[18] A. T. J. B. Eppink and D. H. Parker, Rev. Sci. Instrum. **68**, 3477 (1997).
[19] D. W. Chandler and P. L. Houston, J. Chem. Phys. **87**, 1445 (1987).
[20] A. J. R. Heck and D. W. Chandler, Annu. Rev. Phys. Chem. **46**, 335 (1995).
[21] L. Velarde, T. Habteyes, and A. Sanov, J. Chem. Phys. **125**, 114303 (2006).
[22] E. R. Grumbling, K. Pichugin, R. Mabbs, and A. Sanov, J. Chem. Educ. **88**, 1515 (2011).
[23] V. Dribinski, A. Ossadtchi, V. A. Mandelshtam, and H. Reisler, Rev. Sci. Instrum. **73**, 2634 (2002).
[24] D. M. Neumark, K. R. Lykke, T. Andersen, and W. C. Lineberger, Phys. Rev. A **32**, 1890 (1985).
[25] S. J. Cavanagh, S. T. Gibson, M. N. Gale, C. J. Dedman, E. H. Roberts, and B. R. Lewis, Phys. Rev. A **76**, 052708 (2007).
[26] K. M. Ervin, W. Anusiewicz, P. Skurski, J. Simons, and W. C. Lineberger, J. Phys. Chem. A **107**, 8521 (2003).
[27] F. A. Akin, L. K. Schirra, and A. Sanov, J. Phys. Chem. A **110**, 8031 (2006).
[28] R. Mabbs, F. Mbaiwa, J. Wei, M. Van Duzor, S. T. Gibson, S. J. Cavanagh, and B. R. Lewis, Phys. Rev. A **82**, 011401 (2010).
[29] M. Van Duzor, F. Mbaiwa, J. Wei, T. Singh, R. Mabbs, A. Sanov, S. J. Cavanagh, S. T. Gibson, B. R. Lewis, and J. R. Gascooke, J. Chem. Phys. **133**, 174311 (2010).
[30] T. G. Clements and R. E. Continetti, Phys. Rev. Lett. **89**, 033005 (2002).
[31] J. A. Kelley, W. H. Robertson, and M. A. Johnson, Chem. Phys. Lett. **362**, 255 (2002).
[32] K. A. Hanold, C. R. Sherwood, and R. E. Continetti, J. Chem. Phys. **103**, 9876 (1995).
[33] S. Nandi, A. Sanov, N. Delaney, J. Faeder, R. Parson, and W. C. Lineberger, J. Phys. Chem. A **102**, 8827 (1998).
[34] A. Sanov, T. Sanford, S. Nandi, and W. C. Lineberger, J. Chem. Phys. **111**, 664 (1999).
[35] N. Delaney, J. Faeder, and R. Parson, J. Chem. Phys. **111**, 651 (1999).
[36] L. Sheps, E. M. Miller, S. Horvath, M. A. Thompson, R. Parson, A. B. McCoy, and W. C. Lineberger, Science **328**, 220 (2010).
[37] L. Sheps, E. M. Miller, S. Horvath, M. A. Thompson, R. Parson, A. B. McCoy, and W. C. Lineberger, J. Chem. Phys. **134**, 184311 (2011).
[38] P. H. Krupenie, J. Phys. Chem. Ref. Data **1**, 423 (1972).
[39] A. S. C. Cheung, K. Yoshino, J. R. Esmond, and W. H. Parkinson, J. Mol. Spectrosc. **178**, 66 (1996).